

University of Wisconsin - Madison

MADPH-95-865
CPP-95-1
DOE-ER40757-061
UCD-95-2
RAL-95-003
hep-ph/9501379
January 1995

Probing Strongly-interacting Electroweak Dynamics through W^+W^-/ZZ Ratios at Future e^+e^- Colliders

V. Barger^a, Kingman Cheung^b, T. Han^c and R.J.N. Phillips^d

^a*Physics Department, University of Wisconsin, Madison, WI 53706, USA*

^b*University of Texas at Austin, Center for Particle Physics, Austin, TX 78712, USA*

^c*Physics Department, University of California, Davis, CA 95616, USA*

^d*Rutherford Appleton Laboratory, Chilton, Didcot, Oxon OX11 0QX, UK*

Abstract

We point out that the ratio of $W^+W^- \rightarrow W^+W^-$ and $W^+W^- \rightarrow ZZ$ cross sections is a sensitive probe of the dynamics of electroweak symmetry breaking, in the CM energy region $\sqrt{s_{\text{ww}}} \gtrsim 1$ TeV where vector boson scattering may well become strong. We suggest ways in which this ratio can be extracted at a 1.5 TeV e^+e^- linear collider, using $W^\pm, Z \rightarrow jj$ hadronic decays and relying on dijet mass resolution to provide statistical discrimination between W^\pm and Z . WW fusion processes studied here are unique for exploring scalar resonances of mass about 1 TeV and are complementary to studies via the direct channel $e^+e^- \rightarrow W^+W^-$ for the vector and non-resonant cases. With an integrated luminosity of 200 fb^{-1} , the signals obtained are statistically significant. Comparison with a study of $e^-e^- \rightarrow \nu\nu W^-W^-$ process is made. Enhancements of the signal rate from using a polarized electron beam, or at a 2 TeV e^+e^- linear collider and possible higher energy $\mu^+\mu^-$ colliders, are also presented.

I. Introduction

The mechanism of electroweak symmetry breaking (EWSB) is the foremost open question in particle physics today. One direct approach to this question is to search for Higgs bosons [1]. A complementary approach is to study the scattering of pairs of longitudinally polarized weak bosons [2,3,4] W_L (where and henceforth, W generically denotes W^\pm and Z unless specified otherwise), since at high energies they recall their origins as Goldstone bosons and reflect the EWSB dynamics, thanks to an equivalence theorem [5]. In the Standard Model (SM), if the Higgs boson is not very heavy ($m_H \lesssim 0.5$ TeV), $W_L W_L$ scattering remains relatively weak. But in general, if there is no Higgs boson below about 0.8 TeV, the scattering of W_L pairs is expected to become strong at CM energies of order $\sqrt{s_{\text{ww}}} \gtrsim 1$ TeV. A variety of models of the Strongly-interacting Electro-Weak Sector (SEWS) have been put forward to parameterize this strong scattering, to impose the constraints of unitarity and crossing, and to characterize different EWSB possibilities [2,3,4].

In the present paper we first point out that the cross section ratio $\sigma(W^+W^- \rightarrow W^+W^-)/\sigma(W^+W^- \rightarrow ZZ)$ is a sensitive probe of the SEWS, since different models predict very different ratios. We then suggest ways in which this ratio may be extracted from a “Next e^+e^- Linear Collider” (NLC) with the CM energy $\sqrt{s} = 1.5$ TeV through the W^+W^- fusion processes [6,7,8,9]

$$e^+e^- \rightarrow \bar{\nu}\nu W^+W^-, \bar{\nu}\nu ZZ. \quad (1)$$

In studies of strong WW scattering at hadron colliders, it is necessary for identification to use leptonic W^\pm, Z decays, which have the disadvantages of an invisible neutrino and/or small branching fractions. At e^+e^- colliders we are able to exploit the hadronic decays, which have the advantages of large branching fractions and reconstructibility. Here we rely on $W^\pm, Z \rightarrow jj$ hadronic decays, with sufficient dijet mass resolution to provide statistical discrimination between W^+W^- and ZZ final states. We suggest cuts to minimize the principal backgrounds

from transverse W -pair production that are intrinsic in Eq. (1), and also come from

$$e^+e^- \rightarrow e^+e^-W^+W^-, e^+e^-ZZ, e^\pm\nu W^\mp Z, \quad (2)$$

where the final-state electrons escape undetected along the beam-pipe, as well as from the annihilation channel [10]

$$e^+e^- \rightarrow ZW^+W^- \rightarrow \bar{\nu}\nu W^+W^-. \quad (3)$$

We discuss the prospects for discriminating between W^+W^- , $W^\pm Z$ and ZZ final states and make illustrative calculations to show what may be learned from experiments.

The process $e^-e^- \rightarrow \nu\nu W^-W^-$ is unique to explore the weak “isospin” $I = 2$ non-resonant channel [3,11]. We therefore include a comparison of results at both e^+e^- and e^-e^- colliders. We also show the improvements that would come from using polarized electron beams, in both e^+e^- and e^-e^- cases.

The SEWS effects become significantly larger as energy increases. We therefore demonstrate the enhancement of the signal rate at a 2 TeV e^+e^- collider and possible $\mu^+\mu^-$ circular colliders with larger CM energies [12].

The paper is organized as follows: Section II presents the models to be compared. Section III discusses the question of dijet mass resolution. Section IV describes our methods of calculation and the motivation for our choices of acceptance cuts. Results are presented and discussed in the final two sections. We conclude that at a 1.5 TeV NLC with an integrated luminosity of 200 fb⁻¹, it should be feasible to extract information on SEWS by separately studying W^+W^- and ZZ events.

II. Models for $W_L W_L$ scattering

If we ignore gauge couplings and the mass M_W the scattering of real longitudinal weak bosons $W_L^1 W_L^2 \rightarrow W_L^3 W_L^4$ due to EWSB interactions is the same as the scattering of the corresponding Goldstone bosons [5] and can be parametrized by an amplitude $A(s, t, u)$ as

follows:

$$M(W_L^+ W_L^- \rightarrow Z_L Z_L) = A(s, t, u), \quad (4)$$

$$M(W_L^+ W_L^- \rightarrow W_L^+ W_L^-) = A(s, t, u) + A(t, s, u), \quad (5)$$

$$M(Z_L Z_L \rightarrow Z_L Z_L) = A(s, t, u) + A(t, s, u) + A(u, t, s), \quad (6)$$

$$M(W_L^\pm Z_L \rightarrow W_L^\pm Z_L) = A(t, s, u), \quad (7)$$

$$M(W_L^\pm W_L^\pm \rightarrow W_L^\pm W_L^\pm) = A(t, s, u) + A(u, t, s), \quad (8)$$

where $s = (p_1 + p_2)^2$, $t = (p_1 - p_3)^2$ and $u = (p_1 - p_4)^2$ are the usual Mandelstam variables.

We recall that the amplitudes $T(I)$ for total isospin I , which should obey unitarity, are then given by

$$T(0) = 3A(s, t, u) + A(t, s, u) + A(u, t, s), \quad (9)$$

$$T(1) = A(t, s, u) - A(u, t, s), \quad (10)$$

$$T(2) = A(t, s, u) + A(u, t, s). \quad (11)$$

Unitarity may be monitored through the partial wave amplitudes a_L^I for orbital angular momentum L ,

$$a_L^I = \frac{1}{64\pi} \int_{-1}^1 d(\cos\theta) P_L(\cos\theta) T(I), \quad (12)$$

with $T(I) = 32\pi\Sigma(2L+1)P_L(\cos\theta)a_L^I$. The unitarity condition $|2a_L^I - i| \leq 1$ is sometimes approximated by requiring $|a_L^I| \leq 1$ or $|\text{Re } a_L^I| \leq \frac{1}{2}$.

Various models for these scattering amplitudes have been suggested [2,3,4]. We shall concentrate on models resulting from effective chiral Lagrangians, with and without resonances, as follows.

(a) SM Heavy Higgs Model

The Equivalence Theorem [5] gives the amplitude

$$A(s, t, u) = \frac{-m_H^2}{v^2} \left(1 + \frac{m_H^2}{s - m_H^2 + im_H\Gamma_H\theta(s)} \right), \quad (13)$$

where m_H and Γ_H are the Higgs boson mass and width, $v = 246$ GeV is the usual vacuum expectation value, and $\theta(s) = 1$ (0) for $s > 0$ ($s < 0$). In all models, $A(t, s, u)$ and $A(u, t, s)$ are obtained by permuting s, t, u .

(b) Low-Energy Theorem (LET) Model [13]

This simply extrapolates the amplitudes, prescribed at low energy in terms of v

$$A(s, t, u) = s/v^2, \quad (14)$$

and is the $m_H \rightarrow \infty$ limit of Eq. (13). This model eventually violates unitarity; e.g. a_0^0 violates the bound $|\text{Re } a_0^0| \leq \frac{1}{2}$ when $\sqrt{s} > 1.2$ TeV and the less stringent bound $|a_0^0| \leq 1$ when $\sqrt{s} > 1.7$ TeV, where s denotes the WW invariant mass squared. Our present illustrations scarcely approach these non-unitary ranges. However, at higher energies we can unitarize the amplitudes by a cut-off or by the K -matrix prescription

$$a_L^I \rightarrow a_L^I / (1 - ia_L^I), \quad (15)$$

which enforces the elastic unitarity condition $|2a_L^I - i| = 1$.

(c) Chirally-Coupled Scalar (CCS) Model [4]

This model describes the low-energy behaviour of a technicolor-type model [14] with a techni-sigma scalar resonance, through the amplitude

$$A(s, t, u) = \frac{s}{v^2} - \left(\frac{g_S^2 s^2}{v^2}\right) \frac{1}{s - M_S^2 + iM_S\Gamma_S\theta(s)}, \quad (16)$$

where M_S is the scalar resonance mass and $\Gamma_S = 3g_S^2 M_S^3 / (32\pi v^2)$ is its decay width into Goldstone fields. The SM amplitude with $S = H$ is recovered for $g_S = 1$. We choose $M_S = 1.0$ TeV and $\Gamma_S = 0.35$ TeV, for which $g_S \simeq 0.84$; unsurprisingly, the results are similar to the SM case.

(d) Chirally-Coupled Vector (CCV) Model [4,15]

This model describes the low-energy behaviour of a technicolor-type model [14] with a techni-rho vector resonance V , through the amplitude

$$A(s, t, u) = \frac{s}{4v^2}(4 - 3a) + \frac{aM_V^2}{4v^2} \left[\frac{u - s}{t - M_V^2 + iM_V\Gamma_V\theta(t)} + \frac{t - s}{u - M_V^2 + iM_V\Gamma_V\theta(u)} \right], \quad (17)$$

where M_V and Γ_V are the vector resonance mass and width while $a = 192\pi v^2\Gamma_V/M_V^3$. We choose the case $M_V = 1.0$ TeV with $\Gamma_V = 30$ GeV. Note that the cross section for vector resonance production increases as the width Γ_V becomes larger. The choice of a rather narrow width in our study is motivated from LEP-I constraints via the $Z - V$ mixing [16].

In our signal calculations, we will concentrate on the processes of Eq. (1), which go via the W^+W^- initial state, since the charged current coupling to the electron is larger than the neutral current coupling. We can calculate model (a) directly from the complete SM amplitudes without recourse to the Goldstone boson scattering amplitude $A(s, t, u)$; the latter is shown above simply for comparison. The same is true for model (b), in regions where unitarity is respected. For these two cases, we define the SEWS signals as the excesses of heavy Higgs boson results over that of $m_H = 0$. Models (c) and (d) must however be calculated from the $A(s, t, u)$ expressions, using the Effective W-boson Approximation [17].

We emphasize that the ratio of $W^+W^- \rightarrow W^+W^-$ and $W^+W^- \rightarrow ZZ$ cross sections is a sensitive probe of the SEWS [3], since the models have distinctive particle spectra with different weak isospin content. For a scalar-dominance model, one expects the $W_L^+W_L^-$ rate to be larger than Z_LZ_L ; *e.g.* a SM-like Higgs boson dominating in the s -channel gives $\sigma(H \rightarrow W_L^+W_L^-)/\sigma(H \rightarrow Z_LZ_L) \sim 2$. For a vector-dominance model there would be a significant resonant enhancement in the $W_L^+W_L^-$ mode, but not in Z_LZ_L due to the weak isospin conservation in SEWS (just like $\rho^0 \rightarrow \pi^+\pi^-$ but not $\pi^0\pi^0$ in QCD). On the other hand, if the resonances are far from our reach, then the LET amplitudes behave like $-u/v^2$ for $W_L^+W_L^- \rightarrow W_L^+W_L^-$ and like s/v^2 for $W_L^+W_L^- \rightarrow Z_LZ_L$, so that $\sigma(W_L^+W_L^- \rightarrow Z_LZ_L)/\sigma(W_L^+W_L^- \rightarrow W_L^+W_L^-) = 3/2$. The Z_LZ_L rate is then larger than $W_L^+W_L^-$, and even more so in the central scattering region. Measuring the relative yields of $W_L^+W_L^-$ and Z_LZ_L will therefore reveal important characteristics of the SEWS.

III. Dijet mass resolution

We consider W^\pm and Z bosons detected by their dijet decay modes and identified via the dijet invariant masses $M(W^\pm \rightarrow jj) \simeq M_W$, $M(Z \rightarrow jj) \simeq M_Z$. With realistic mass resolution, discrimination cannot be made event-by-event but can be achieved on a statistical basis.

The experimental W dijet mass distributions will contain the intrinsic decay widths folded with experimental resolution factors depending on calorimetry and geometry. We have explored the possible dijet mass resolution using two alternative jet energy resolution algorithms [18]

$$\delta E_j/E_j = 0.50/\sqrt{E_j} \oplus 0.02 \quad \text{Algorithm A} \quad (18)$$

$$= 0.25/\sqrt{E_j} \oplus 0.02 \quad \text{Algorithm B} \quad (19)$$

in GeV units, where the symbol \oplus means adding in quadrature. We applied this to the typical SM background process $e^+e^- \rightarrow e^+\nu W^-Z$ at $\sqrt{s} = 1.5$ TeV, averaging over all final $W \rightarrow jj$ dijet decays with gaussian smearing of jet energies according to these algorithms; the resulting $W^\pm \rightarrow jj$ and $Z \rightarrow jj$ dijet invariant mass distributions are shown in Fig. 1. Since this study omits angular resolution effects, sensitive to details of detector design, we shall adopt the more conservative algorithm A for further illustrations.

If we now identify dijets having measured mass in the intervals

$$[0.85M_W, \frac{1}{2}(M_W + M_Z)] \quad \text{and} \quad [\frac{1}{2}(M_W + M_Z), 1.15M_Z]$$

as $W^\pm \rightarrow jj$ and $Z \rightarrow jj$, respectively, algorithm A indicates that true W^+W^- , $W^\pm Z$, $ZZ \rightarrow jjjj$ events will be interpreted statistically as follows:

$$WW \Rightarrow 78\% WW, 18\% WZ, 1\% ZZ, 3\% \text{ reject,}$$

$$WZ \Rightarrow 11\% WW, 77\% WZ, 9\% ZZ, 3\% \text{ reject,}$$

$$ZZ \Rightarrow 2\% WW, 22\% WZ, 72\% ZZ, 4\% \text{ reject,}$$

These numbers show that misidentification of W^+W^- as ZZ (or vice versa) is very unlikely; also the loss of W^+W^- or ZZ signal strength is not in itself very serious. The principal

danger comes from $W^\pm Z$ events that are misidentified as W^+W^- or ZZ , confusing or even swamping these signals if $W^\pm Z$ production is relatively large. We must therefore ensure, via suitable acceptance criteria, that $W^\pm Z$ production is not an order of magnitude bigger than W^+W^- or ZZ signal.

A final caveat: the numbers above refer strictly to light-quark jets. In b - and c -quark jets there is an appreciable probability of $b \rightarrow cl\nu$ and/or $c \rightarrow sl\nu$ ($\ell = e, \mu$ or τ) semileptonic decays, where neutrinos deplete the visible jet energy. Thus more $Z \rightarrow jj$ dijets will be interpreted as $W^\pm \rightarrow jj$, but *not* vice versa. We have modeled this effect in typical situations with Scenario A and find that the correction to the $W^\pm \rightarrow jj$ results is rather small. However, about 8% more $W^\pm Z$ events are now identified as W^+W^- (increasing this source of background); also about 10% more ZZ events are now identified as $W^\pm Z$ (increasing this loss of signal). These changes are significant but not disastrous. The resulting modified identification probabilities are as follows:

$$\begin{aligned}
WW &\Rightarrow 73\% WW, \quad 17\% WZ, \quad 1\% ZZ, \quad 9\% \text{ reject}, \\
WZ &\Rightarrow 19\% WW, \quad 66\% WZ, \quad 7\% ZZ, \quad 8\% \text{ reject}, \\
ZZ &\Rightarrow 5\% WW, \quad 32\% WZ, \quad 55\% ZZ, \quad 8\% \text{ reject},
\end{aligned}$$

and we will use these numbers in the rest of our analyses.

When the dijet mass resolution function is known, for a given detector, the apparent W^+W^- , $W^\pm Z$ and ZZ rates can be unfolded to determine approximately the underlying true rates. In the following, we first concentrate our attention on these true rates, and then use the examples above to estimate resolution effects.

IV. SM calculations and acceptance cuts

The SM signals for $W_L^+W_L^- \rightarrow W_L^+W_L^-$, $Z_L Z_L$ fusion processes with a heavy Higgs boson have been considered previously, along with certain SM backgrounds [6,7,8,9]. The irreducible SM backgrounds to the Strongly-interacting Electro-Weak Sector, which include transversely

polarized vector bosons W_T^\pm and Z_T production, can be obtained by setting $m_H = 0$; further backgrounds arise from misidentifying other SM channels in Eq. (2).

We first address the annihilation background of Eq. (3), which has different dynamics and requires different cuts from the other backgrounds. It is important at $\sqrt{s} = 0.5$ TeV [8], but unlike the scattering channels, its cross section increases slowly with \sqrt{s} above the threshold and then decreases after $\sqrt{s} \sim 1$ TeV, like $1/s$ asymptotically. At $\sqrt{s} = 1.5$ TeV the total annihilation background cross section is of order 10 fb (taking into account three flavors of the neutrinos from the Z decay), comparable to the SEWS signals. It can be reduced severely, however, by a cut on the recoil mass M_{recoil} that is the invariant mass of all the final-state particles excluding the $W^+W^- \rightarrow (jj)(jj)$ system:

$$M_{\text{recoil}}^2 = s + M_{WW}^2 - 2\sqrt{s}(E_{W^+} + E_{W^-}), \quad (20)$$

where the W boson energies E_W are defined in the e^+e^- CM frame and \sqrt{s} is the CM energy of the e^+e^- collider. The recoil-mass spectrum of the annihilation Eq. (3) peaks at M_Z , due to the $Z \rightarrow \nu\bar{\nu}$ decay, but this peak is smeared out by the contributions of initial-state radiation as well as the mismeasurement of the W hadronic energies. A cut such as

$$M_{\text{recoil}} > 200 \text{ GeV}, \quad (21)$$

therefore effectively suppresses the annihilation background. Figure 2 shows that this background is reduced to about 1–2% of typical SEWS signals, with negligible effect on the scattering channels at $\sqrt{s} = 1.5$ TeV. We shall henceforth make this cut and neglect the annihilation background of Eq. (3).

The remaining scattering cross sections of interest are illustrated in Fig. 3. This figure shows SM cross sections for the fusion processes with both $m_H = 0$ (solid curves) and $m_H = 1$ TeV (dashed curves); the excess over the $m_H = 0$ case represents the SEWS signal in the SM Heavy Higgs Model. The SEWS signals of present interest have final-state $W_L^+W_L^-$ and Z_LZ_L pairs, giving four-jet final states with two undetected neutrinos [see Eq. (1)]; the branching fractions for four-jet decays are not included in this section.

We start with the most basic acceptance cuts. Since we are interested in WW scattering at high subprocess energy, we look for pairs of weak bosons with high invariant masses M_{WW} , high transverse momenta $p_T(W)$ of the vector bosons, and relatively large angles θ_W with respect to the beam axis. We require

$$M_{WW} > 500 \text{ GeV} ; \quad p_T(W) > 150 \text{ GeV} ; \quad |\cos \theta_W| < 0.8. \quad (22)$$

The solid curves in Fig. 4 show the resulting cross sections at $\sqrt{s} = 1.5 \text{ TeV}$ in (a) the W^+W^- channel and (b) the ZZ channel, for the SM Heavy Higgs Model ($m_H = 1 \text{ TeV}$) and the LET Model ($m_H = \infty$); SM backgrounds are also shown. Note that the solid curves represent sums of signal plus the intrinsic background; the signals alone are found by subtracting the $m_H = 0$ curve, in this and subsequent figures.

Figure 4 immediately illustrates the main point of this paper, that the W^+W^-/ZZ signal ratio is sensitive to the details of SEWS; we see that the SM Heavy Higgs model ($m_H = 1 \text{ TeV}$) gives $W^+W^-/ZZ > 1$ whereas the LET Model ($m_H = \infty$) gives $W^+W^-/ZZ < 1$. It also shows that the ZZ signals around $M_{ZZ} \sim 1 \text{ TeV}$ are bigger than the backgrounds, since Section III indicates that the W^+W^- background has very small ($\sim 1\%$) probability to be misidentified as ZZ , but more work is needed to separate the W^+W^- signals.

The SM $e^+e^-W^+W^-$ background gets very large contributions from the virtual $\gamma\gamma \rightarrow W^+W^-$ subprocess, which gives mainly dibosons with small net transverse momentum $p_T(WW)$, quite unlike the SEWS signal and other backgrounds. Figure 5 compares the W^+W^- signals and backgrounds versus $p_T(WW)$, after the first-level cuts of Eqs. (21)–(22); it shows the small- p_T peak of $e^+e^-W^+W^-$, and also shows how the W_T backgrounds are favored at very large p_T . It is clearly advantageous to select an intermediate range of $p_T(WW)$, to remove a lot of background at little cost to the signal; we make somewhat similar cuts for $p_T(ZZ)$, though these are less crucial. Specifically we require

$$50 \text{ GeV} < p_T(WW) < 300 \text{ GeV}, \quad 20 \text{ GeV} < p_T(ZZ) < 300 \text{ GeV}, \quad (23)$$

at $\sqrt{s} = 1.5 \text{ TeV}$. With large minimum $p_T(WW)$ and $p_T(ZZ)$ requirements, it becomes

much less likely that the final-state electrons in $eeWW$ and $e\nu WZ$ background channels can escape undetected down the beam-pipes; a veto on visible hard electrons is now very effective against $eeWW$ (less so against $e\nu WZ$). We therefore impose the veto [7]

$$\text{no } e^\pm \text{ with } E_e > 50 \text{ GeV and } |\cos\theta_e| < \cos(0.15 \text{ rad}) \quad (24)$$

Figure 6 compares the resulting $m_H = 1 \text{ TeV}$ (SM) and $m_H = \infty$ (LET) cross sections with backgrounds at $\sqrt{s} = 1.5 \text{ TeV}$, versus diboson invariant mass, after imposing all the above cuts. Combining these results with the typical $WW \Rightarrow ZZ$ and $WZ \Rightarrow WW, ZZ$ misidentification probabilities from Section III, we see that both SEWS model signals are now observable over the total remaining SM backgrounds. We henceforth adopt the cuts of Eqs. (21)–(24) and present detailed results in the next section.

The lowest order backgrounds $e^+e^- \rightarrow W^+W^-, ZZ$ can be removed by the cuts on $p_T(WW)$ and M_{recoil} . We have neglected QCD backgrounds from $e^+e^- \rightarrow jjjj$ production. They are formally of order $\alpha^2\alpha_s^2$ compared to our electroweak cross sections of order α^4 , but the QCD 4-jet final states contain no direct neutrino production and will be heavily suppressed by the M_{recoil} and $p_T(WW)$ cuts; they will be further suppressed by the $M(jj) \simeq M_W, M_Z$ requirements. We have also neglected $e^+e^- \rightarrow \bar{t}t \rightarrow \bar{b}bW^+W^-$ as a source of background; this gives unwanted extra jets and would be suppressed by the $p_T(WW)$ cut if the b-jets escaped near the beam axis.

V. Results

Table I presents our results for e^+e^- collisions at $\sqrt{s} = 1.5 \text{ TeV}$, showing signal and background cross sections before and after successive cuts. Here the SM Heavy Higgs and LET Model signals have been found by subtracting the SM $m_H = 0$ intrinsic background from SM $m_H = 1 \text{ TeV}$ and $m_H = \infty$ values, respectively. Partial wave unitarity is respected at all energies reached so that no unitarization needs to be imposed [19]. For the chirally coupled scalar (CCS) and chirally coupled vector (CCV) models, the signals are calculated in the

Table I: Cross sections in fb, before and after cuts, for e^+e^- collisions at $\sqrt{s} = 1.5$ TeV. For comparison, results for $e^-e^- \rightarrow \nu\nu W^-W^-$ are also presented, with the same energy and the W^+W^- cuts. Hadronic branching fractions of WW decays and the W^\pm/Z identification/misidentification are not included here. The first number in the final $e^+e^-W^+W^-$ and $e\nu WZ$ entries denotes the $p_T > 20$ GeV choice, for the case where WW and WZ are misidentified as ZZ ; the second number (in parentheses) denotes the $p_T > 50$ GeV choice, for the case where they are identified as WW .

Contribution	no cuts	with Eqs. (21)–(22)	with Eqs. (21)–(24)
$\bar{\nu}\nu W^+W^-$ signals (fb)			
SM ($m_H = 1$ TeV)	7.7	3.5	2.4
CCS ($M_S, \Gamma_S = 1, 0.35$ TeV)	–	3.5	2.4
CCV ($M_V, \Gamma_V = 1, 0.03$ TeV)	–	1.5	1.0
LET ($m_H = \infty$)	3.1	0.61	0.46
$\bar{\nu}\nu ZZ$ signals (fb)			
SM ($m_H = 1$ TeV)	5.9	2.4	2.2
CCS ($M_S, \Gamma_S = 1, 0.35$ TeV)	–	2.7	2.5
CCV ($M_V, \Gamma_V = 1, 0.03$ TeV)	–	0.72	0.67
LET ($m_H = \infty$)	3.4	0.89	0.84
$\nu\nu W^-W^-$ signals (fb)			
SM ($m_H = 1$ TeV)	2.7	0.53	0.39
CCS ($M_S, \Gamma_S = 1, 0.35$ TeV)	–	0.71	0.52
CCV ($M_V, \Gamma_V = 1, 0.03$ TeV)	–	0.72	0.53
LET ($m_H = \infty$)	3.5	0.89	0.63
SM Backgrounds (fb)			
$\bar{\nu}\nu W^+W^-$ ($m_H = 0$)	45	1.1	0.86
$\bar{\nu}\nu ZZ$ ($m_H = 0$)	18	0.84	0.72
$e^+e^-W^+W^-$ ($m_H = 0$)	2000	28	3.5(0.95)
$e\nu WZ$ ($m_H = 0$)	150	4.6	3.1(2.7)
$e^-e^- \rightarrow \nu\nu W^-W^-$ ($m_H = 0$)	51	2.3	1.7

Effective W -boson Approximation [17]. The validity of this approximation can be checked by comparing CCS (with $g_S = 1$) to the exact SM results; there is agreement at the 20% level, using the cuts in Eq. (22). In such an approximation, however, the kinematical cuts of Eqs. (23)–(24) cannot be implemented; we have therefore assumed the efficiencies of these cuts to be the same as for the SM heavy Higgs boson ($m_H = 1$ TeV) signal. For comparison, results for $e^-e^- \rightarrow \nu\nu W^-W^-$ are also included [11], with the same cuts as the $\bar{\nu}\nu W^+W^-$ case. We remark that the LET signal rates for $e^+e^- \rightarrow \nu\bar{\nu}ZZ$ and $e^-e^- \rightarrow \nu\nu W^-W^-$ channels are essentially equal (when the cuts imposed are the same); this is a consequence of the Low Energy Theorem and crossing symmetry for $W_L W_L$ scattering. Branching fractions for $W \rightarrow jj$ decays and W^\pm/Z identification/misidentification factors are not included in this table.

In Fig. 7 we present the expected signal and background event rates versus diboson mass for different models at a 1.5 TeV NLC, assuming an integrated luminosity of 200 fb⁻¹. The branching fractions $BR(W \rightarrow jj) = 67.8\%$ and $BR(Z \rightarrow jj) = 69.9\%$ [20] and the W^\pm/Z identification/misidentification factors (final set of Section III) are all included here. Comparing the W^+W^- events (Fig. 7a) and ZZ events (Fig. 7b), we once again see that a broad Higgs-like scalar will enhance both W^+W^- and ZZ channels with $\sigma(W^+W^-) > \sigma(ZZ)$; a ρ -like vector resonance will manifest itself through W^+W^- but not ZZ ; while the LET amplitude will enhance ZZ more than W^+W^- . Table II summarizes the corresponding total signal S and background B event numbers, summing over diboson invariant mass bins, together with the statistical significance S/\sqrt{B} . The LET signal for W^+W^- is particularly small; the ratio S/B can be enhanced by making a higher mass cut (e.g. $M_{WW} > 0.7$ TeV), but the significance S/\sqrt{B} is not in fact improved by this. Results for $e^-e^- \rightarrow \nu\nu W^-W^-$ have again been included for comparison.

At the NLC, since electron polarization of order 90–95% at injection with only a few percent depolarization during acceleration may well be achievable [21], it is interesting to consider also the effects of beam polarization. The $W^+W^- \rightarrow W^+W^-$, ZZ scattering signals

of interest arise from initial e_L^- and e_R^+ states only and the signal cross sections are therefore doubled with an e_L^- beam. Table III(a) shows the background cross sections for the beams $e^+e_L^-$, $e^-e_L^-$ and $e_L^-e_L^-$. Based on these results, event numbers and significances for the case of 100% e_L^- beam at $\sqrt{s} = 1.5$ TeV with 200 fb^{-1} are shown in Table III(b), to be compared with Table II; S and B for intermediate beam polarizations can be found by interpolating Table II and Table III.

Table II: Total numbers of W^+W^- , $ZZ \rightarrow 4\text{-jet}$ signal S and background B events calculated for a 1.5 TeV NLC with integrated luminosity 200 fb^{-1} . Events are summed over the mass range $0.5 < M_{WW} < 1.5$ TeV except for the W^+W^- channel with a narrow vector resonance in which $0.9 < M_{WW} < 1.1$ TeV. The statistical significance S/\sqrt{B} is also given. For comparison, results for $e^-e^- \rightarrow \nu\nu W^-W^-$ are also presented, for the same energy and luminosity and the W^+W^- cuts. The hadronic branching fractions of WW decays and the W^\pm/Z identification/misidentification are included.

channels	SM $m_H = 1 \text{ TeV}$	Scalar $M_S = 1 \text{ TeV}$	Vector $M_V = 1 \text{ TeV}$	LET
$S(e^+e^- \rightarrow \bar{\nu}\nu W^+W^-)$	160	160	46	31
$B(\text{backgrounds})$	170	170	4.5	170
S/\sqrt{B}	12	12	22	2.4
$S(e^+e^- \rightarrow \bar{\nu}\nu ZZ)$	120	130	36	45
$B(\text{backgrounds})$	63	63	63	63
S/\sqrt{B}	15	17	4.5	5.7
$S(e^-e^- \rightarrow \nu\nu W^-W^-)$	27	35	36	42
$B(\text{backgrounds})$	230	230	230	230
S/\sqrt{B}	1.8	2.3	2.4	2.8

Since the SEWS signals increase with CM energy, a 2 TeV e^+e^- linear collider would give a larger signal rate. We find (see Fig. 3) that at $\sqrt{s} = 2$ TeV the $m_H = 1$ TeV and

Table III: Improvements from using 100% polarized e_L^- beams in a 1.5 TeV e^+e^-/e^-e^- collider. Part (a) gives SM background cross sections in fb with the full cuts Eqs. (21)–(24); the signal cross sections are simply doubled with each e_L^- beam compared to Table I. Part (b) gives the expected numbers of signal and background events for integrated luminosity 200 fb^{-1} , to be compared with Table II.

(a) SM Backgrounds	Cross sections in fb with Eqs. (21)–(24)			
$e^+e_L^- \rightarrow \bar{\nu}\nu W^+W^- (m_H = 0)$	1.7			
$e^+e_L^- \rightarrow \bar{\nu}\nu ZZ (m_H = 0)$	1.4			
$e^+e_L^- \rightarrow e^+e^-W^+W^- (m_H = 0)$	4.3 (1.3)			
$e^+e_L^- \rightarrow e\nu WZ (m_H = 0)$	4.5 (3.9)			
$e^-e_L^- \rightarrow \nu\nu W^-W^- (m_H = 0)$	3.4			
$e^-e_L^- \rightarrow e^-e^-W^+W^- (m_H = 0)$	1.3			
$e^-e_L^- \rightarrow e^-e^-W^-Z (m_H = 0)$	4.4			
$e_L^-e_L^- \rightarrow \nu\nu W^-W^- (m_H = 0)$	6.8			
$e_L^-e_L^- \rightarrow e^-e^-W^+W^- (m_H = 0)$	1.8			
$e_L^-e_L^- \rightarrow e^-e^-W^-Z (m_H = 0)$	6.5			

(b) channels	SM	Scalar	Vector	LET
	$m_H = 1 \text{ TeV}$	$M_S = 1 \text{ TeV}$	$M_V = 1 \text{ TeV}$	
$S(e^+e^- \rightarrow \bar{\nu}\nu W^+W^-)$	330	320	92	62
$B(\text{backgrounds})$	280	280	7.1	280
S/\sqrt{B}	20	20	35	3.7
$S(e^+e^- \rightarrow \bar{\nu}\nu ZZ)$	240	260	72	90
$B(\text{backgrounds})$	110	110	110	110
S/\sqrt{B}	23	25	6.8	8.5
$S(e^-e_L^- \rightarrow \nu\nu W^-W^-)$	54	70	72	84
$B(\text{background})$	400	400	400	400
S/\sqrt{B}	2.7	3.5	3.6	4.2
$S(e_L^-e_L^- \rightarrow \nu\nu W^-W^-)$	110	140	140	170
$B(\text{background})$	710	710	710	710
S/\sqrt{B}	4.0	5.2	5.4	6.3

$m_H = \infty$ signal cross sections are, for W^+W^- ,

$$\sigma_{\text{SEWS}}(\text{SM } 1\text{TeV}) = \sigma_{W^+W^-}(m_H = 1 \text{ TeV}) - \sigma_{W^+W^-}(m_H = 0) \simeq 20 \text{ fb}$$

$$\sigma_{\text{SEWS}}(\text{LET}) = \sigma_{W^+W^-}(m_H = \infty) - \sigma_{W^+W^-}(m_H = 0) \simeq 5 \text{ fb}$$

and for ZZ ,

$$\sigma_{\text{SEWS}}(\text{SM } 1\text{TeV}) = \sigma_{ZZ}(m_H = 1 \text{ TeV}) - \sigma_{ZZ}(m_H = 0) \simeq 14 \text{ fb}$$

$$\sigma_{\text{SEWS}}(\text{LET}) = \sigma_{ZZ}(m_H = \infty) - \sigma_{ZZ}(m_H = 0) \simeq 7 \text{ fb}$$

The signal rates are enhanced by about a factor ~ 2 – 2.5 by increasing the CM energy from 1.5 to 2 TeV (compared with the first numerical column in Table I).

It may be more advantageous to study the SEWS at possible higher energy $\mu^+\mu^-$ colliders [12]. To demonstrate this point, Fig. 8 gives the \sqrt{s} -dependence of the corresponding SM total cross sections for $m_H = 1$ TeV as well as the various backgrounds (with $m_H = 0$). The excesses over the $m_H = 0$ case again represent the SEWS signals in the SM Heavy Higgs Model. We see that the uncut $\bar{\nu}\nu W^+W^-$ and $\bar{\nu}\nu ZZ$ signals increase most rapidly at the lower energies; starting from the NLC values at $\sqrt{s} = 1.5$ TeV, they have increased by factors ~ 2 – 2.5 at $\sqrt{s} = 2$ TeV and by factors ~ 10 at $\sqrt{s} = 4$ TeV (the value currently being discussed for a possible $\mu^+\mu^-$ circular collider [12]). More detailed considerations would depend on design parameters of the collider and detector; in the absence of firm information, we do not pursue this question any further here [22].

Finally we note that our calculated cross sections and event rates neglect bremsstrahlung and beamstrahlung initial state radiation, which somewhat reduce the effective CM energy and with it the signal and principal backgrounds. Colliders are usually designed to minimize beamstrahlung. The net corrections are expected to be small and our general conclusions are not affected.

VI. Summary and Discussion

Our main results are summarized in Fig. 7 and Tables II–III for an e^+e^- collider at

$\sqrt{s} = 1.5$ TeV. They show that the W^+W^-/ZZ event ratio is a sensitive probe of SEWS dynamics. Indeed, the differences between the various models are quite marked and the observation of such signals would provide strong indications about the underlying dynamics of the SEWS. In fact, not only the ratio but also the size of the separate W^+W^- and ZZ signals contains valuable dynamical information. Our results show statistically significant signals for a 1 TeV scalar or vector state. We also find a 5.7σ signal for the LET amplitudes via the $W^+W^- \rightarrow ZZ$ channel alone without the improvement by beam polarization. Our event numbers are based on optimized acceptance cuts and a luminosity 200 fb^{-1} , roughly corresponding to one year running with a favorable design [21,23].

Our approach is based on $W^+W^-, ZZ \rightarrow (jj)(jj)$ four-jet signals, and therefore relies on good dijet mass resolution. Our simulations included energy resolution but not angular resolution, being conservative about the former to compensate for our neglect of the latter; we also folded in the effects of finite W and Z widths and of semileptonic decays in b - and c -quark jets. We therefore believe that our final W^\pm/Z identification/misidentification factors are not unrealistic.

For an e^-e^- collider with the same energy and luminosity, the LET signal rate for the $\nu\nu W^-W^-$ ($I = 2$) channel is similar to the LET result of $e^+e^- \rightarrow \bar{\nu}\nu ZZ$, as anticipated, while the background rate is higher.

The signals are doubled for an e_L^- polarized beam (or quadrupled for two e_L^- beams), whereas the backgrounds increase by smaller factors. Hence polarization improves the significance of signals substantially, for given luminosity: compare Tables II and III.

The signals also increase strongly with the CM energy. A 2 TeV e^+e^- linear collider would increase the signal rates by roughly a factor of 2–2.5. If future $\mu^+\mu^-$ colliders can reach higher energies with comparable luminosities and comparable signal/background discrimination, an order of magnitude increase in signal rate may be expected at $\sqrt{s} = 4$ TeV: see Fig. 8.

By way of further discussion, we offer the following comments and comparisons.

(a) It may be possible to exploit $ZZ \rightarrow (jj)(\ell^+\ell^-)$ signals, to confirm the hadronic ZZ

results. The former have smaller branching fraction (reducing both signal and intrinsic background by a factor 0.19), but the $WZ \Rightarrow ZZ$ misidentification background is reduced by a factor 0.1 and the W^+W^- backgrounds are eliminated. It may also be possible to exploit b -tagging to improve the discrimination between W^\pm and Z dijets. Since 39% of all $ZZ \rightarrow (jj)(jj)$ events contain at least one $b\bar{b}$ jet pair, and b -tagging efficiencies of 30–40% per event can be contemplated, requiring a tag would reduce the $ZZ \rightarrow 4j$ signal and intrinsic backgrounds by a factor 0.12–0.16; in comparison, WZ events would be reduced by 0.066–0.088 and W^+W^- backgrounds would be eliminated.

(b) The direct s -channel process $e^+e^- \rightarrow W^+W^-$ should be more advantageous in searching for effects from a vector V through $\gamma, Z - V$ mixing [15,16,23,24], due to more efficient use of the CM energy, the known beam energy constraint, and better control of backgrounds. However, the WW fusion processes studied here involve more spin-isospin channels of WW scattering; they are unique for exploring scalar resonances and are complementary to the direct s -channel for the vector and non-resonant cases.

(c) The conclusions of Ref. [25] are pessimistic about studying the LET amplitude ($m_H \rightarrow \infty$) at a 1.5 TeV NLC via the $\bar{\nu}\nu W^+W^-$ channel; in contrast, we find that the NLC has significant potential to explore non-resonant SEWS physics, reaching about a 5.7σ signal for one-year running in the $\bar{\nu}\nu ZZ$ channel alone. The improvement comes mainly from including the $W^+W^- \rightarrow ZZ$ process and from our optimized kinematical cuts to suppress the backgrounds while maximally preserving the SEWS signal.

(d) We have concentrated on $\nu\bar{\nu}W^+W^-, \nu\bar{\nu}ZZ$ final states, neglecting $e\nu WZ$ signals, because the heavy Higgs boson contribution to the latter is negligibly small compared to the irreducible SM background (see Fig. 3). However, the presence of an $I = 1$ vector state would greatly enhance the cross section for $e^+e^- \rightarrow e^\pm\nu W^\mp Z$ [25]. Our optimal kinematical cuts and the $M(jj)$ reconstruction should be essentially applicable to the WZ channel and a wider study including this channel would provide consistency checks on SEWS effects.

(e) The LET amplitudes we employed correspond to the lowest order universal term in the

energy expansion in effective chiral Lagrangians [26]. The magnitude and sign of coefficients of higher dimension operators (the so-called anomalous couplings) in the Lagrangians would depend on specific SEWS models. In the clean environment at the NLC, one may be able to measure the shape as well as the normalization of the WW mass distribution rather well. If this can be achieved, one may even hope to study the non-resonance amplitudes in detail to go beyond the LET term and to extract the underlying dynamics at higher mass scales beyond $\mathcal{O}(1 \text{ TeV})$.

(f) Finally, in studying a scalar or a vector resonance, we have followed the simplest approach of assuming just one resonance at a time. It has been emphasized recently [27] that there may coexist several resonances (as in low energy QCD), a scalar (σ -like), a vector (ρ -like), an axial vector (a_1 -like) and an isospin-singlet vector (ω -like), obeying some algebraic relations to satisfy the proper Regge behavior and certain sum rules of strong scattering [28]. There would be definite relations among the masses and couplings of these resonances, leading to cancellation and other predictions in the strong scattering amplitudes. This possibility deserves further scrutiny in studying SEWS effects at colliders.

Acknowledgments

We thank Tim Barklow, Dave Burke and Ron Ruth for helpful conversations on many NLC issues. We are grateful to Jonathan Feng, Jon Guy and Bill Scott for discussions about dijet mass resolution. This work has been supported in part by Department of Energy Grants DE-FG03-91ER40674, DOE-FG03-93ER40757 and DE-FG02-95ER40896, and in part by the University of Wisconsin Research Committee with funds granted by the Wisconsin Alumni Research Foundation. T.H. is also supported in part by a UC-Davis Faculty Research Grant.

References

- [1] For a review see J.F. Gunion, H.E. Haber, G.L. Kane and S. Dawson, “The Higgs Hunter’s Guide” (Addison-Wesley, Reading, MA 1990).
- [2] M. Chanowitz, in *Perspectives on Higgs Physics*, edited by G. Kane (World Scientific, 1992), p. 343; and references therein; K. Hikasa, in *Physics and Experiments with Linear Collider*, Saariselka, Finland 1991, edited by R. Orava, P. Eerola and M. Nordberg (World Scientific, Singapore, 1992); and references therein.
- [3] T. Han, in proceedings of *Physics and Experiments with Linear e^+e^- Colliders*, ed. by F. Harris *et al.*, World Scientific (1993); and references therein.
- [4] J. Bagger *et al.*, Phys. Rev. **D49**, 1246 (1994); and references therein.
- [5] J.M. Cornwall, D.N. Levin and G. Tiktopoulos, Phys. Rev. **D10**, 1145 (1974); B.W. Lee, C. Quigg and H.B. Thacker, Phys. Rev. **D16**, 1519 (1977); M.S. Chanowitz and M.K. Gaillard, Nucl. Phys. **B261**, 379 (1985).
- [6] J. Gunion and A. Tofighi-Niaki, Phys. Rev. **D36**, 2671 (1987); *ibid* **38**, 1433 (1988).
- [7] K. Hagiwara, J. Kanzaki and H. Murayama, KEK-TH-282 (1991).
- [8] V. Barger, K. Cheung, B.A. Kniehl and R.J.N. Phillips, Phys. Rev. **D46**, 3725 (1992).
- [9] Y. Kurihara and R. Najima, Phys. Lett. **B301**, 292 (1993).
- [10] V. Barger and T. Han, **212**, 117 (1988); V. Barger, T. Han and R. Phillips, Phys. Rev. **D39**, 146 (1989); A. Tofighi-Niaki and J. Gunion, Phys. Rev. **D39**, 720 (1989).
- [11] V. Barger, J. Beacom, K. Cheung and T. Han, Phys. Rev. **D50**, 6704 (1994).
- [12] See *Proceedings of the Physics Potential and Development of $\mu^+\mu^-$ Colliders Workshop*, Sausalito, CA, November 1994, D. Cline, editor (to be published).

- [13] S. Weinberg, Phys. Rev. Lett. **17**, 616 (1966); M. S. Chanowitz, M. Golden and H. Georgi, Phys. Rev. Lett. **57**, 2344 (1986); Phys. Rev. **D35** 1149 (1987).
- [14] For a modern review on Technicolor theories, see K. Lane, BUHEP-94-2, Lectures given at the Theoretical Advanced Studies Institute, University of Colorado, Boulder, to appear in the 1993 TASI Lectures (World Scientific); and references therein.
- [15] R. Casalbuoni et al., Phys. Lett. **B155**, 95 (1985); Nucl. Phys. **B282**, 235 (1987); see also M. Bando, T. Kugo, and K. Yamawaki, Phys. Rep. **164**, 217 (1988); and references therein.
- [16] R. Casalbuoni et al., Phys. Lett. **B269**, 361 (1991).
- [17] M. S. Chanowitz and M. K. Gaillard, Phys. Lett. **B142**, 85 (1984); G. L. Kane, W. W. Repko and W. R. Rolnick, Phys. Lett. **B148**, 367 (1984); S. Dawson, Nucl. Phys. **B249**, 42 (1985).
- [18] A. Miyamoto, in proceedings of *JLC Workshop*, Tsukuba, 1990.
- [19] We have employed the simple Breit-Wigner form for the Higgs boson propagator with its tree-level width. This prescription, however, may violate unitarity at the heavy Higgs boson resonance and the cross section may be overestimated by about 20%. See, *e. g.*, S. Willenbrock and G. Valencia, Phys. Lett. **B247**, 341 (1990).
- [20] Particle Data Group, Phys. Rev. **D50**, No.3 (1994).
- [21] T. Barklow, D. Burke and Ron Ruth, private communication.
- [22] For related discussions at $\mu^+\mu^-$ colliders, see V. Barger, J. Gunion, and T. Han, in preparation.
- [23] T. Barklow, talk presented at Albuquerque DPF 94, SLAC-PUB-6618; and references therein.

- [24] M. E. Peskin, in *Physics and Experiments with Linear Colliders*, Saariselkä, Finland, Sept., 1992, ed. R. Orava *et al.*; and references therein.
- [25] Y. Kurihara and R. Najima, KEK-PREPRINT-93-90; and in *Proceedings of the fourth workshop on Japan Linear Collider*, KEK Proceedings 94-1, p.20, edi. Y. Kurihara.
- [26] A. Dobado and M. Herrero, Phys. Lett. **B228**, 495 (1989); A. Dobado, M. Herrero and J. Terron, Z. Phys. **C50**, 205 (1991); S. Dawson and G. Valencia, Nucl. Phys. **B352**, 27 (1991); J. Bagger, S. Dawson and G. Valencia, Nucl. Phys. **B399**, 364 (1993).
- [27] S. Weinberg, Phys. Rev. Lett. **65**, 1177 (1990); T. Han, Z. Huang and P.Q. Hung, LBL—36270 (1994).
- [28] F. Gilman and H. Harari, Phys. Rev. **165**, 1803 (1968); and references therein.

Figure captions

Fig. 1: $W^\pm \rightarrow jj$ and $Z \rightarrow jj$ dijet invariant mass distributions for $e^+e^- \rightarrow e\nu WZ$ events at $\sqrt{s} = 1.5$ TeV, found by applying (a) algorithm A and (b) algorithm B (see text) for calorimeter energy resolution, omitting angular resolution and heavy-quark decay effects.

Fig. 2: SM $e^+e^- \rightarrow \bar{\nu}\nu W^+W^-$ annihilation and scattering cross sections versus M_{recoil} at $\sqrt{s} = 1.5$ TeV. Annihilation (dotted curve) is compared to scattering with $m_H = 1$ TeV (solid curve) and $m_H = 0$ (dashed curve).

Fig. 3: Cross sections for SM scattering processes that can contribute SEWS signals and backgrounds in the $e^+e^- \rightarrow \bar{\nu}\nu W^+W^-$ and $\bar{\nu}\nu ZZ$ channels, versus CM energy \sqrt{s} .

Fig. 4: SEWS signal and background cross sections versus diboson invariant mass at $\sqrt{s} = 1.5$ TeV, after the first-level cuts of Eqs. (21)–(22), in the channels (a) $e^+e^- \rightarrow \bar{\nu}\nu W^+W^-$ and (b) $e^+e^- \rightarrow \bar{\nu}\nu ZZ$. Solid curves denote total SM contributions with $m_H = 1$ TeV (Heavy Higgs Model) and with $m_H = \infty$ (LET Model); dotted curves denote intrinsic SM backgrounds ($m_H = 0$). Dashed and dot-dashed curves show $eeWW$ and $e\nu WZ$ production. $W^\pm, Z \rightarrow jj$ branching fractions and W^\pm/Z identification/misidentification factors are not included.

Fig. 5: W^+W^- signal and background cross sections versus transverse momentum $p_T(WW)$ after the first-level cuts of Eqs. (21)–(22). Solid curves denote total contributions from the SM Heavy Higgs Model (with $m_H = 1$ TeV) and the LET Model (with $m_H = \infty$); other curves denote backgrounds as in Fig. 4. $W^\pm, Z \rightarrow jj$ branching fractions and W^\pm/Z identification/misidentification factors are not included.

Fig. 6: SEWS signal and background cross sections versus diboson invariant mass at $\sqrt{s} = 1.5$ TeV, after the combined cuts of Eqs. (21)–(24): (a) in the W^+W^- channel and (b) in the ZZ channel. Notation follows Fig. 4. $W^\pm, Z \rightarrow jj$ branching fractions and W^\pm/Z identification/misidentification factors are not included.

Fig. 7: Expected numbers of $W^+W^-, ZZ \rightarrow (jj)(jj)$ signal and background events, in 20 GeV bins of diboson invariant mass, for 200 fb^{-1} luminosity at $\sqrt{s} = 1.5$ TeV: (a) W^+W^- events, (b) ZZ events. Dijet branching fractions and W^\pm/Z identification/misidentification factors are included. The dotted histogram denotes total SM background including misidentifications. The solid, dashed and dot-dashed histograms denote signal plus background for the LET, SM and CCV models, respectively; CCS model results are close to the SM case.

Fig. 8: Cross sections for SM scattering processes that contribute SEWS signals and backgrounds in the $\mu^+\mu^- \rightarrow \bar{\nu}\nu W^+W^-$ and $\bar{\nu}\nu ZZ$ channels, versus CM energy \sqrt{s} .

This figure "fig1-1.png" is available in "png" format from:

<http://arxiv.org/ps/hep-ph/9501379v1>

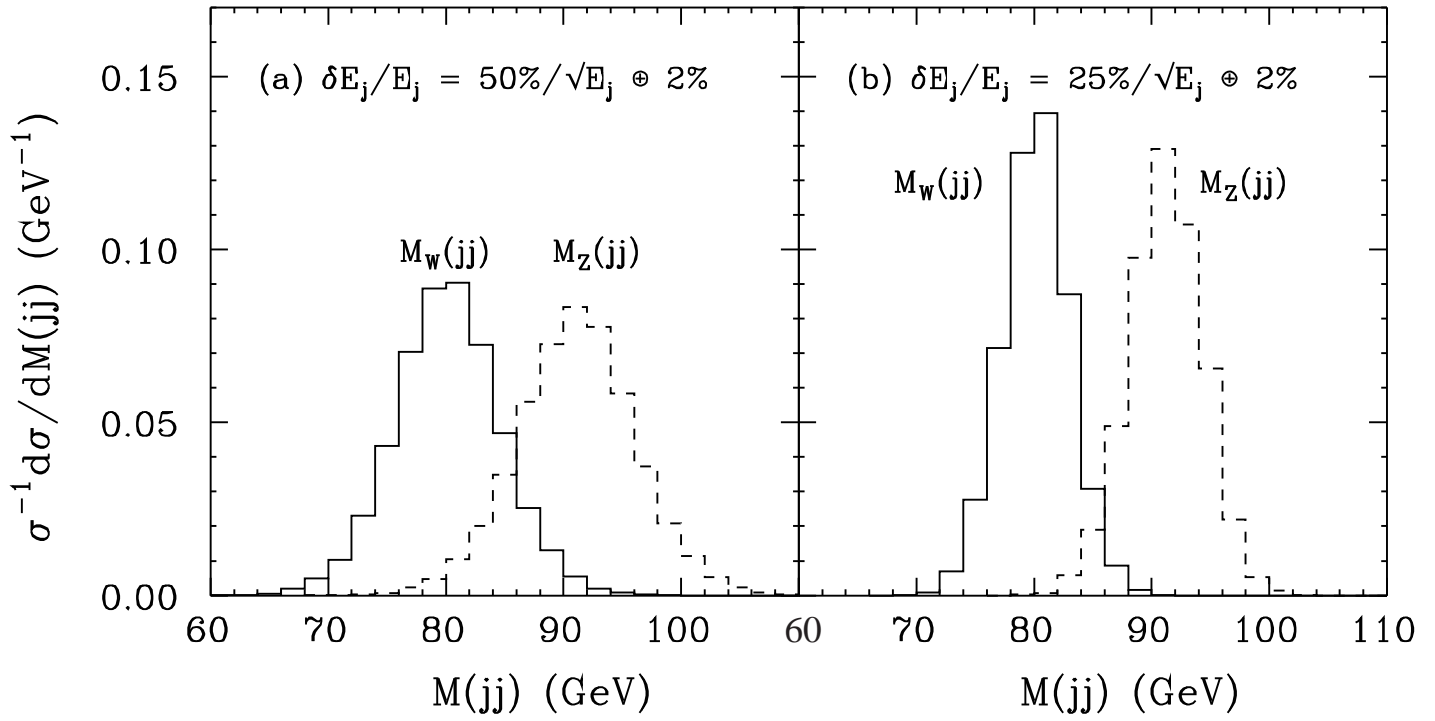


Fig. 1

This figure "fig1-2.png" is available in "png" format from:

<http://arxiv.org/ps/hep-ph/9501379v1>

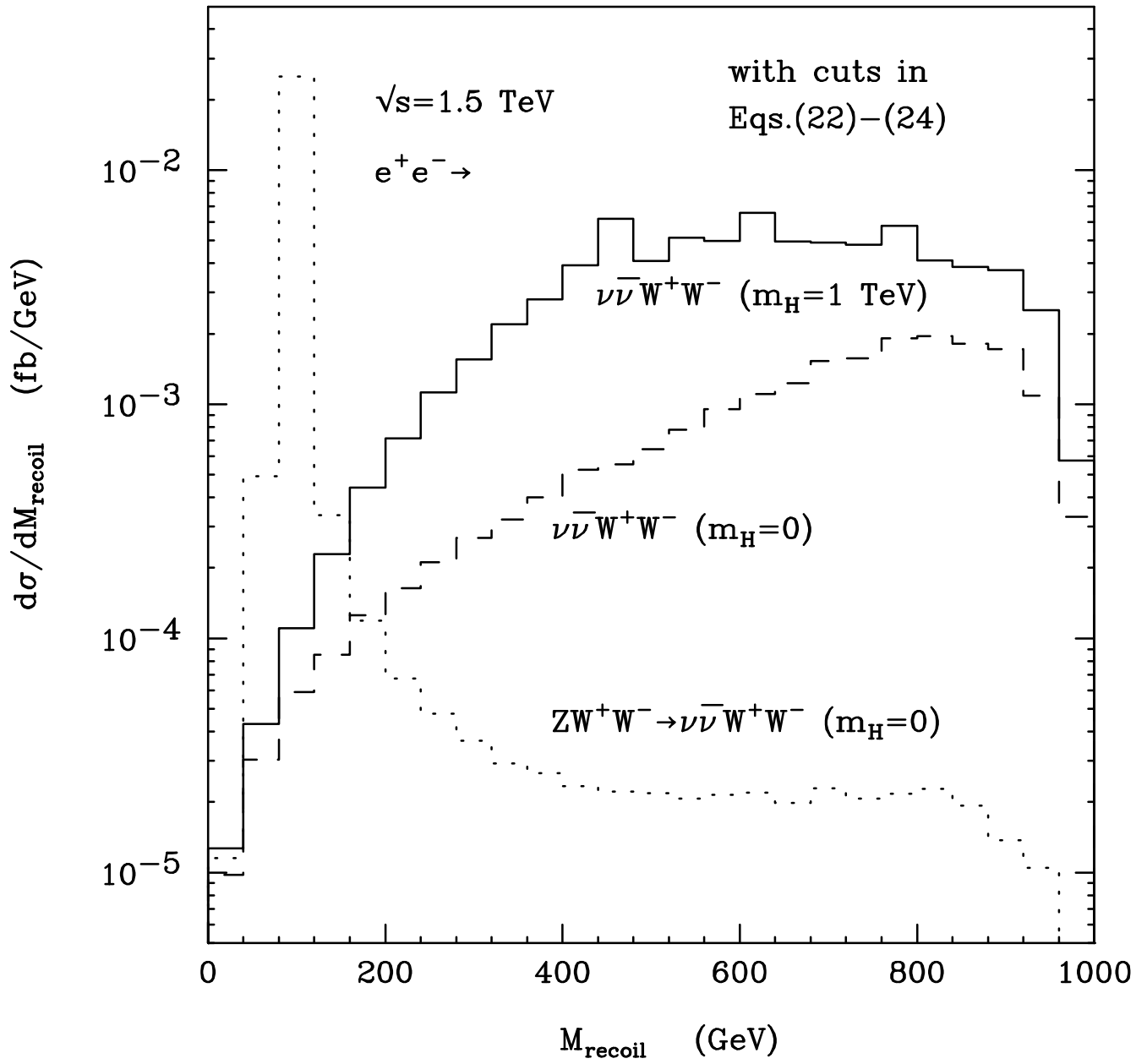


Fig. 2

This figure "fig1-3.png" is available in "png" format from:

<http://arxiv.org/ps/hep-ph/9501379v1>

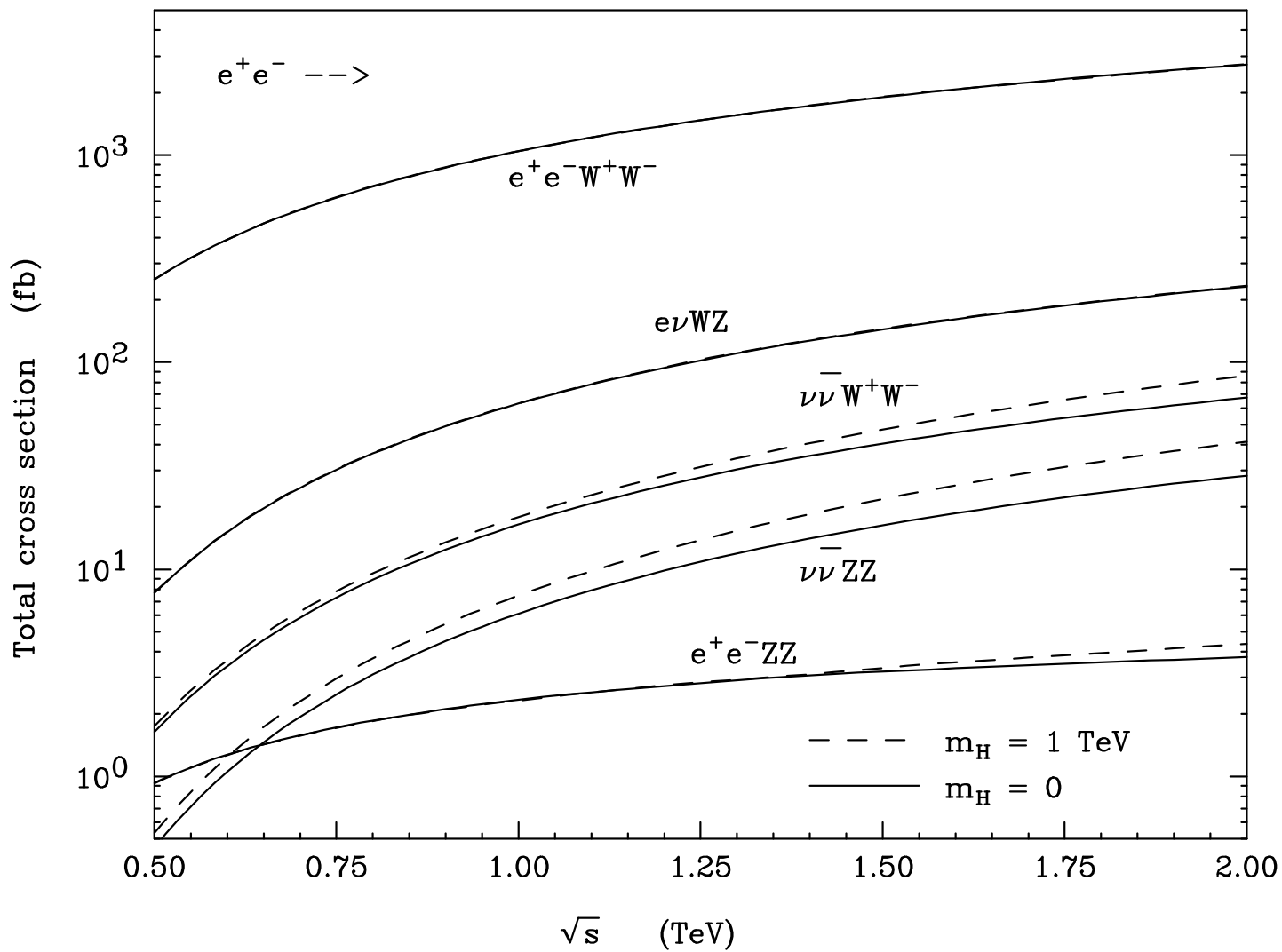


Fig. 3

This figure "fig1-4.png" is available in "png" format from:

<http://arxiv.org/ps/hep-ph/9501379v1>

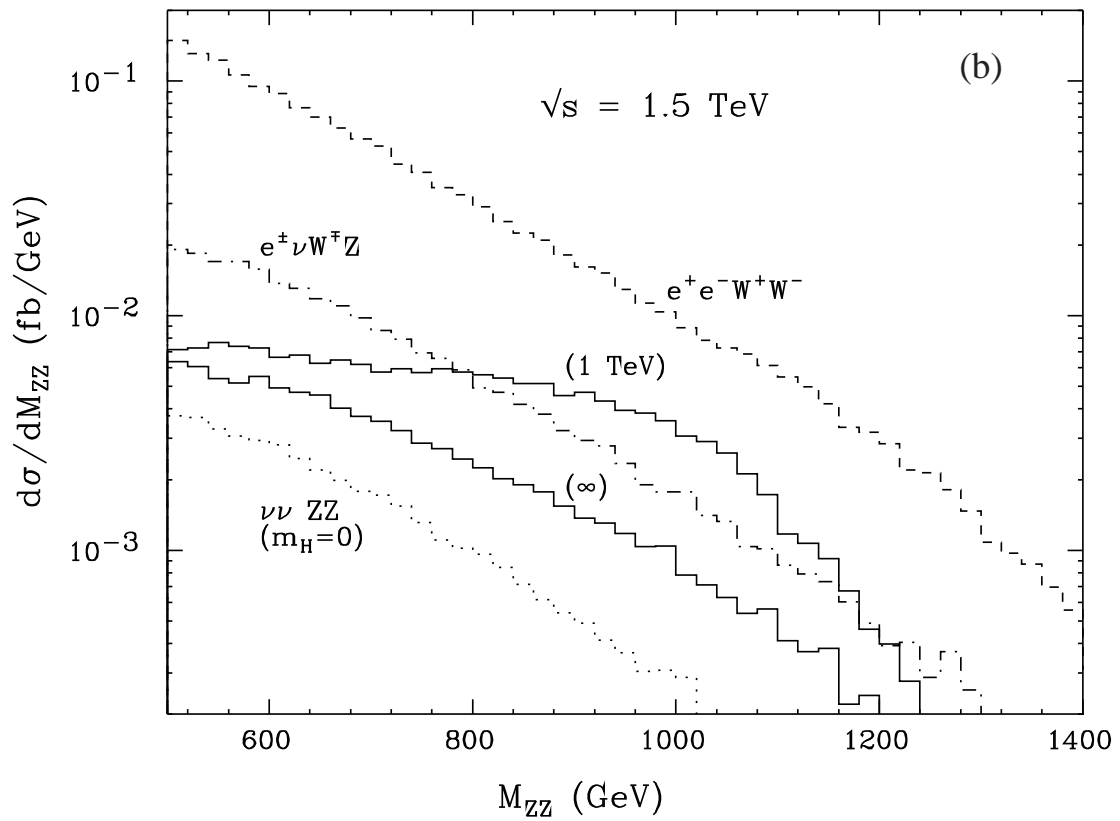
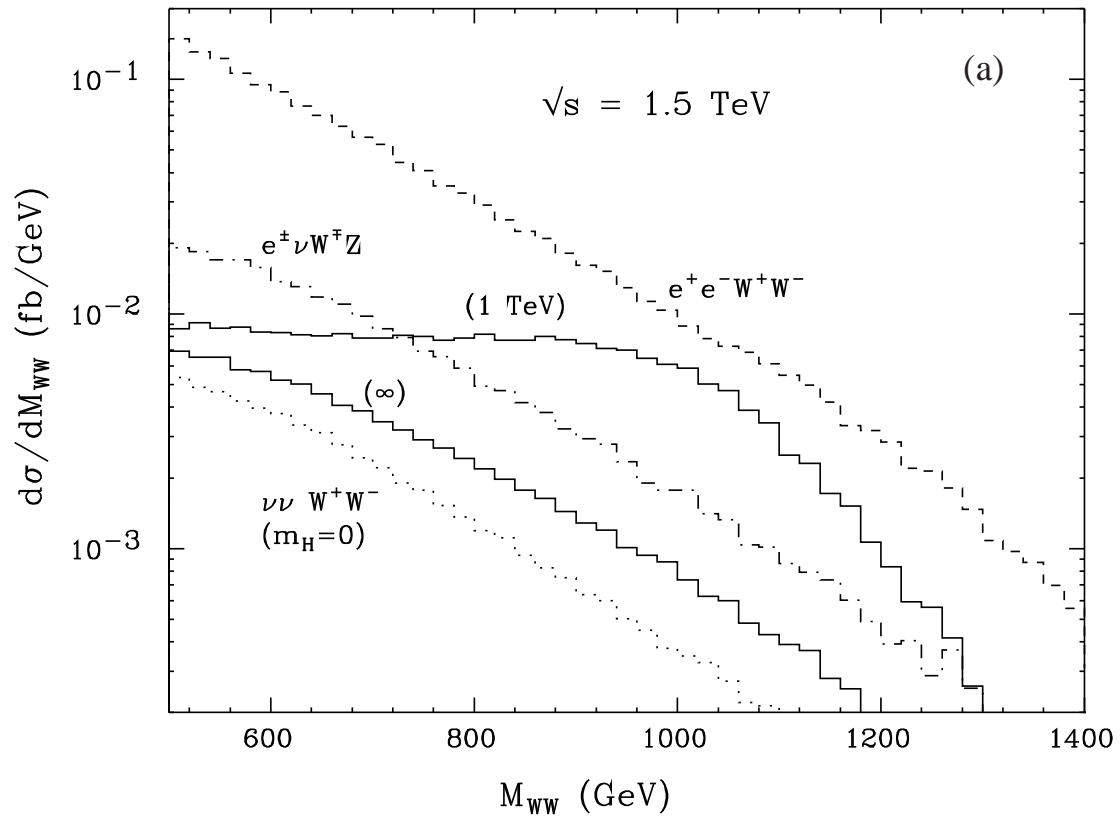


Fig. 4

This figure "fig1-5.png" is available in "png" format from:

<http://arxiv.org/ps/hep-ph/9501379v1>

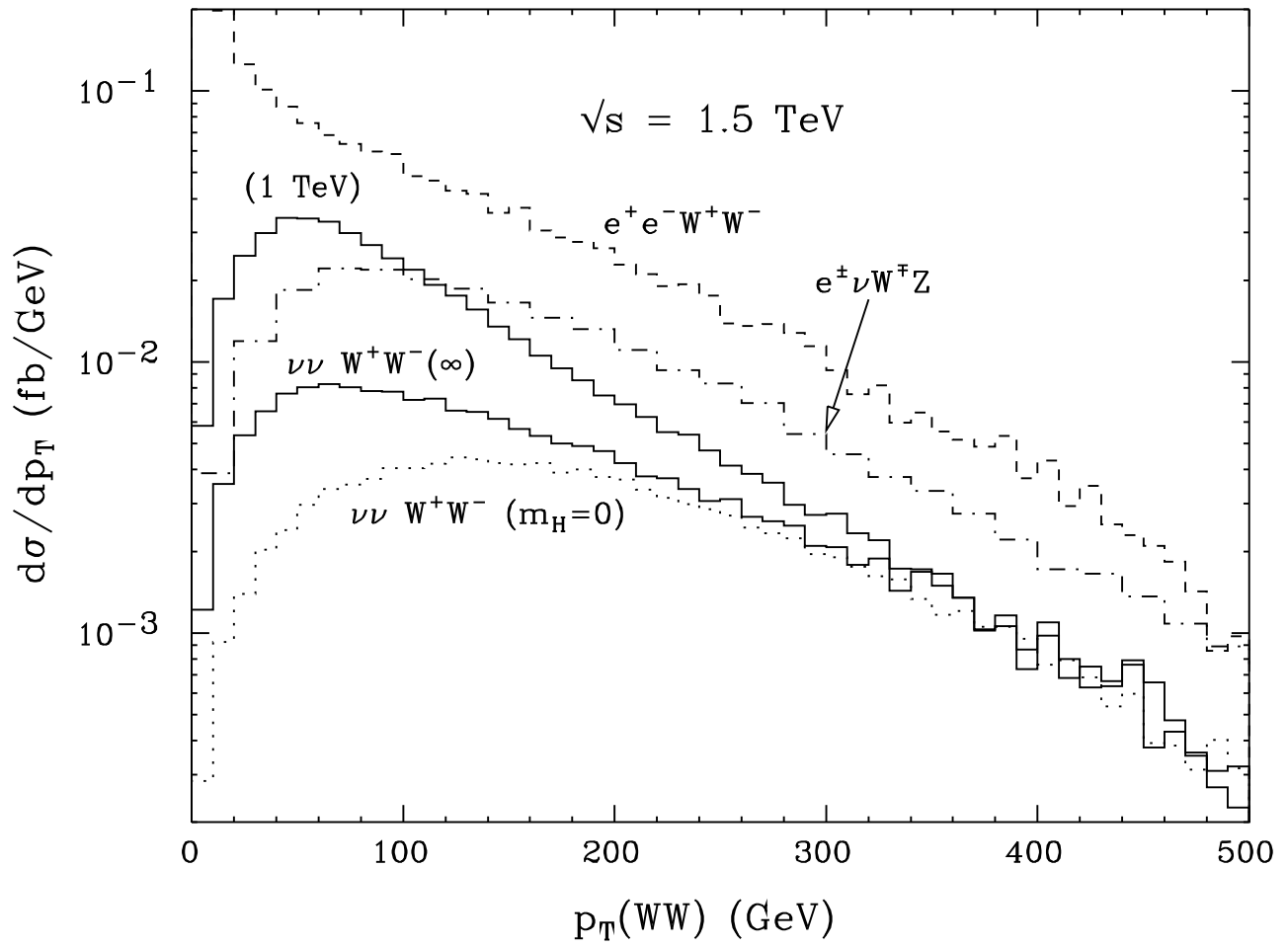


Fig. 5

This figure "fig1-6.png" is available in "png" format from:

<http://arxiv.org/ps/hep-ph/9501379v1>

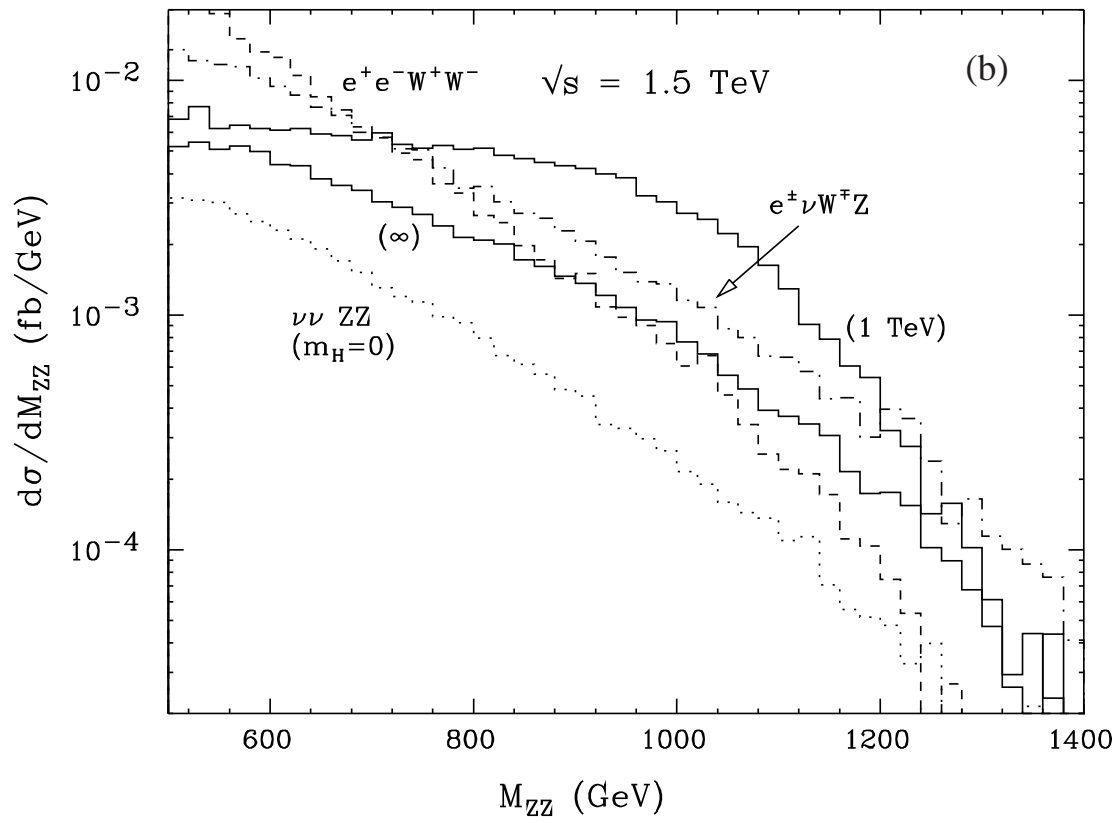
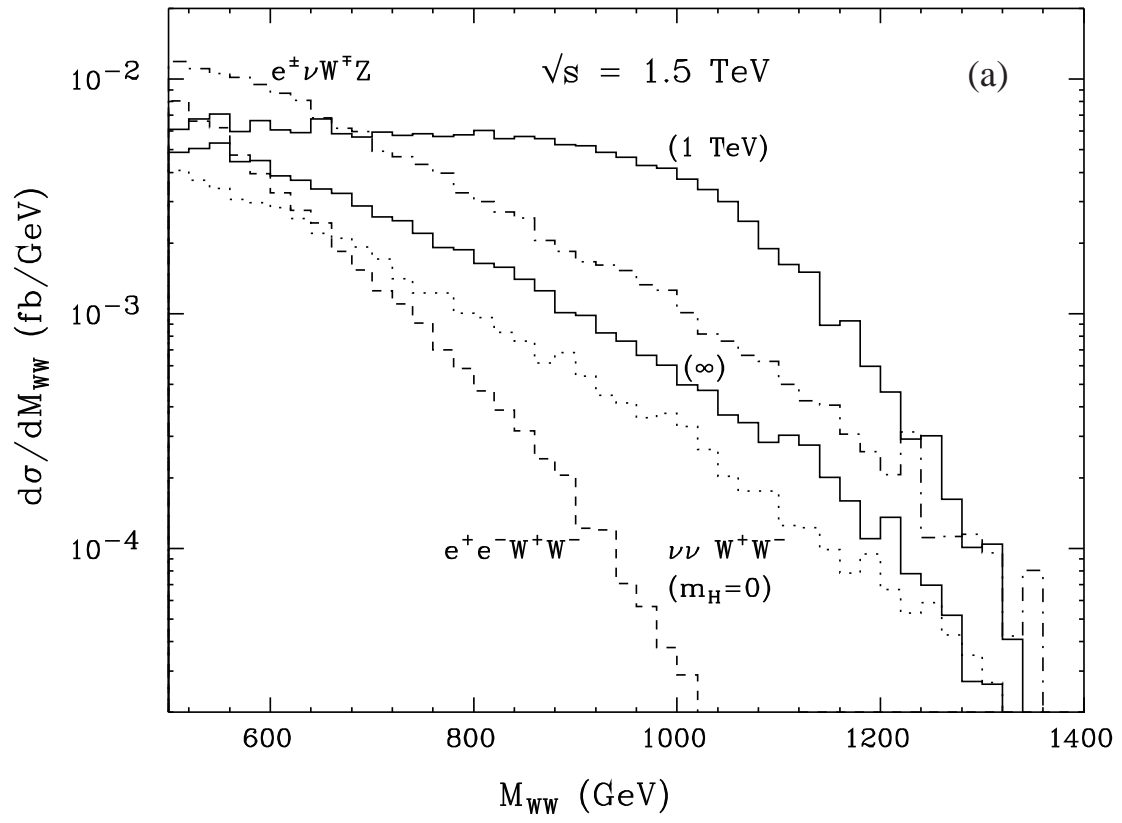


Fig. 6

This figure "fig1-7.png" is available in "png" format from:

<http://arxiv.org/ps/hep-ph/9501379v1>

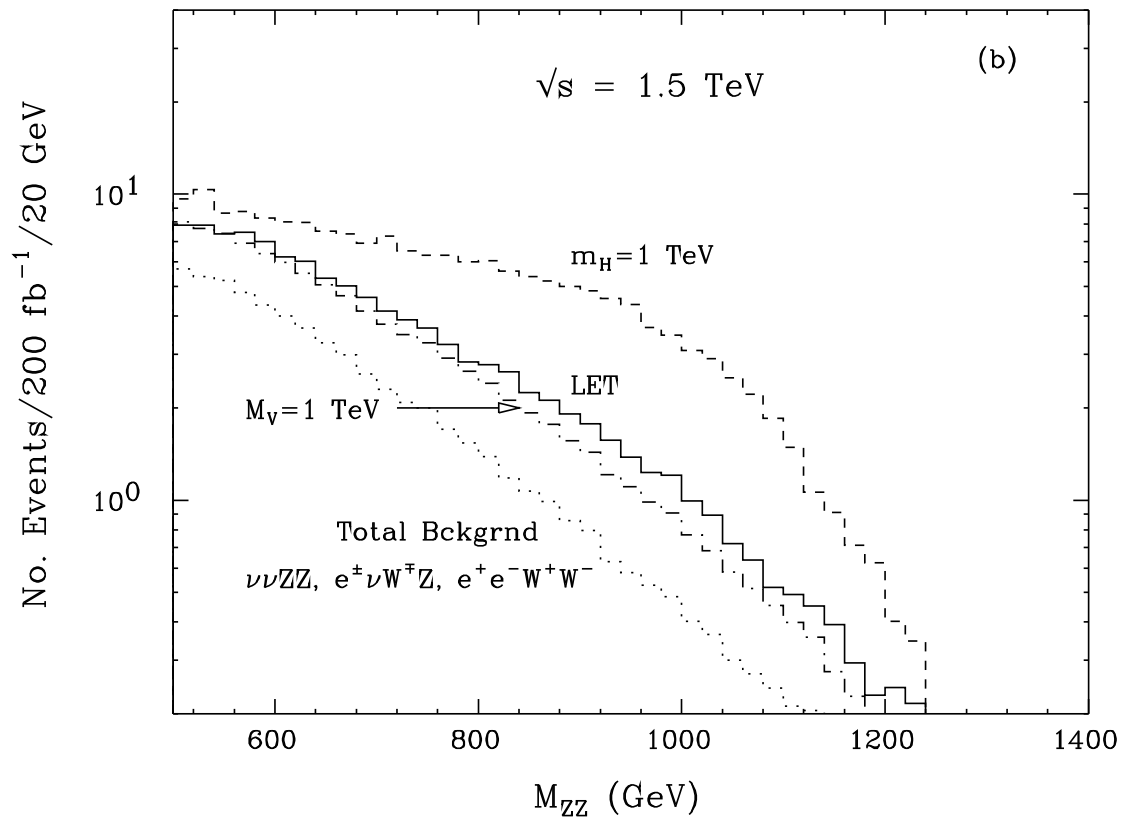
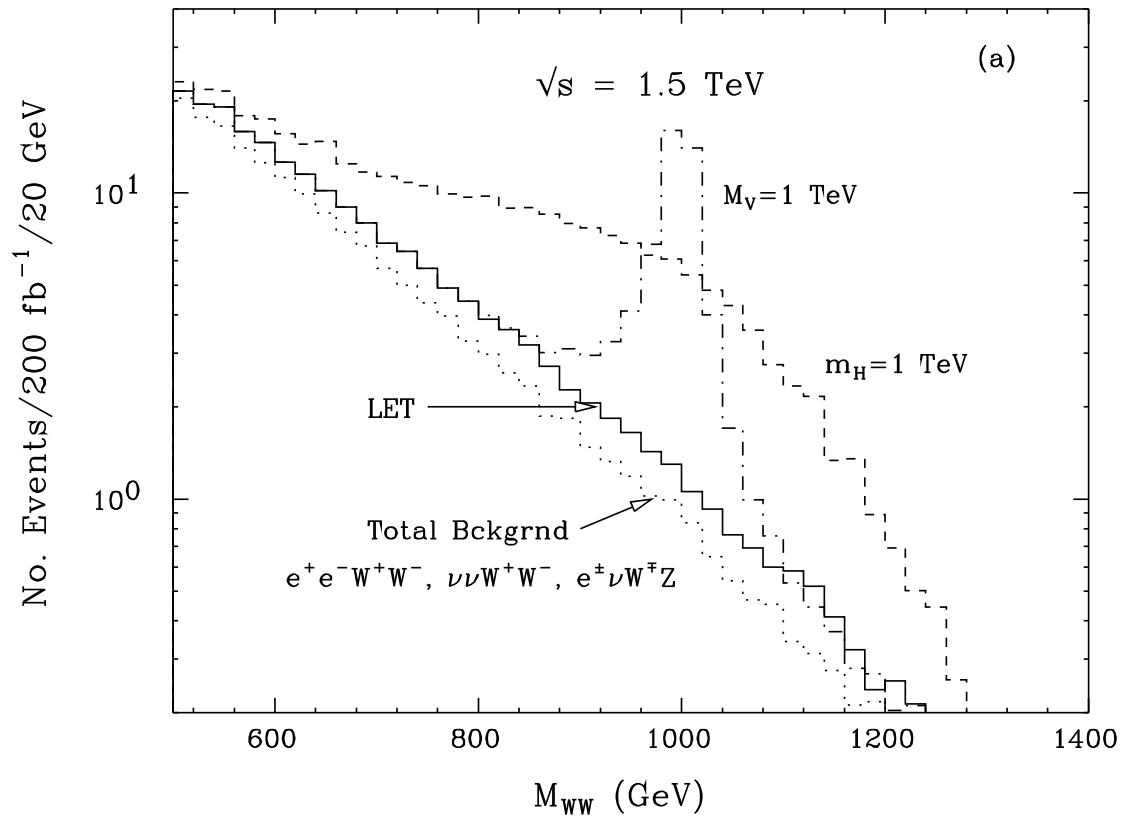


Fig. 7

This figure "fig1-8.png" is available in "png" format from:

<http://arxiv.org/ps/hep-ph/9501379v1>

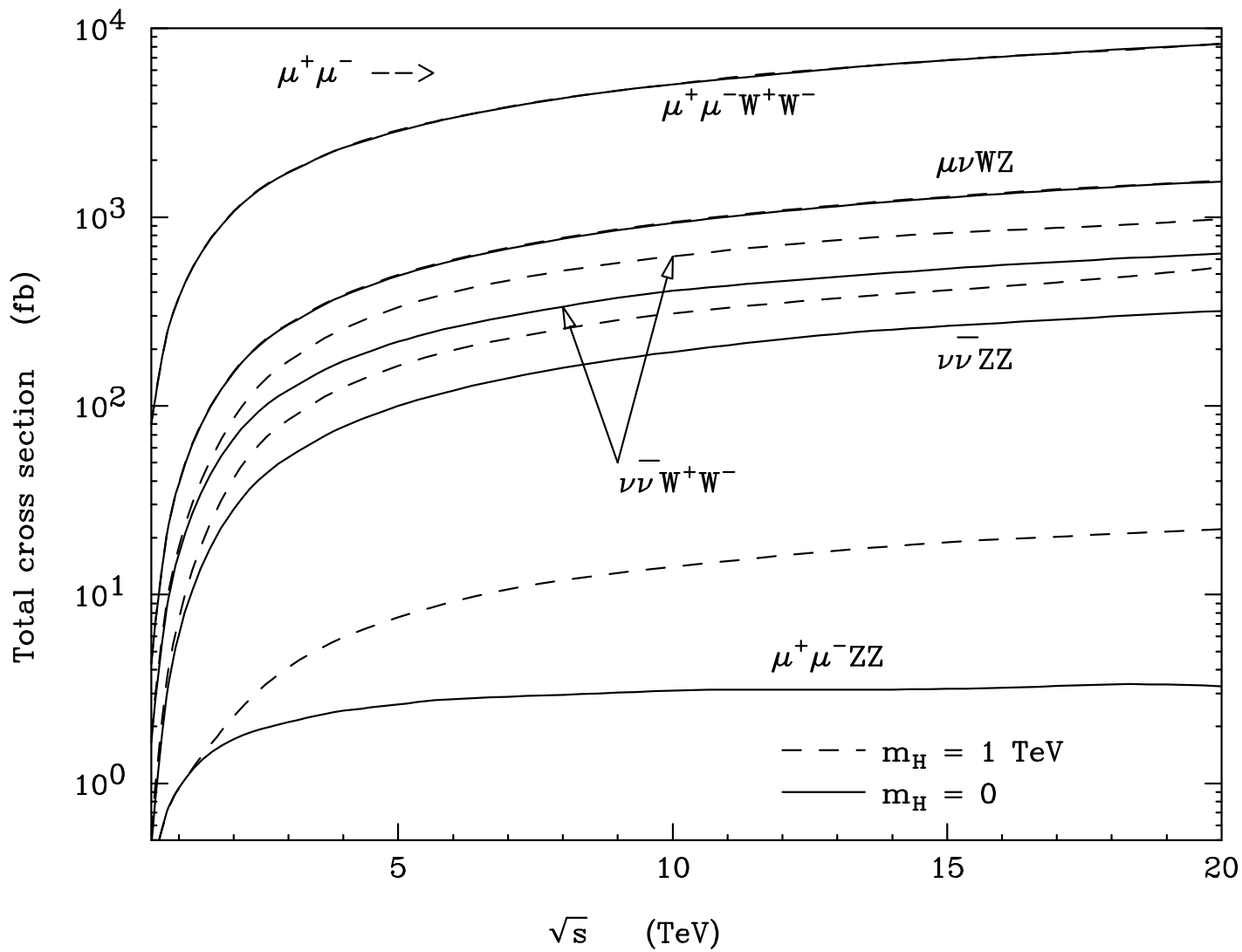


Fig. 8